Portugaliae Electrochimica Acta 2020, 38(1), 43-58

DOI: 10.4152/pea.202001043

PORTUGALIAE ELECTROCHIMICA ACTA
ISSN 1647-1571

Exploring the Capability of Synthesized PVP-Oxime for Corrosion Inhibition of a Mild Steel Surface in a 1 M H_2SO_4 Solution

Nisha Saini[a], Rajeev Kuma[a], Priti Pahuja[a], Reena Malik[a], Rinki Malik[a], Sushila Singhal[b] and Suman Lata[a,*]

[a] *Department of Chemistry, Deenbandhu Chhotu Ram University of Science and Technology, Murthal (131039), Haryana, India*
[b] *Department of Chemistry, Deshbandhu College, University of Delhi, New Delhi, 110019, India*

Received September 8, 2017; accepted April 30, 2018

Abstract

Polyvinylpyrrolidone Oxime (PVPO) was synthesized and studied for mild steel (MS) corrosion inhibition in 1 M H_2SO_4, at different concentrations and temperatures. The corrosion inhibition efficiency was studied using weight loss method, polarization technique, electrochemical impedance spectroscopy (EIS), scanning electron microscopy (SEM) and quantum chemical calculations. The results from weight loss, potentiodynamic polarization and EIS showed that the inhibition efficiency (I. E.) increased with gradual increments in the inhibitor concentration, and decreased at higher temperatures. The polarization study also revealed that PVPO acted as a mixed type inhibitor, and Langmuir adsorption isotherm fitted well for the adsorption behavior. The highest corrosion efficiency was found to be 88.39%, with a concentration of 1000 ppm, and a temperature of 303 K. The corrosion inhibition mechanism has been further proposed, including the support from the theoretical study. SEM images also verified the MS surface smoothening in PVPO presence, and, hence, it has shown to be a good corrosion inhibitor.

***Keywords**:* mild steel, PVPO, corrosion inhibition, adsorption, thermodynamic study.

Introduction

Mild steel (MS) is highly applicable in various industries, as well as to domestic purposes, due to its accordable characteristics and affordable costs. Although it is used for the fabrication of various reaction vessels, pipes, tanks, etc., it shows considerable limitations, because it gets corroded during various industrial processes, such as acid pickling and cleaning, oil well acidizing, etc., which results in MS degradation. This process depends upon MS conditions and

* Corresponding author. E-mail address: sumanjakhar.chem@dcrustm.org

temperature, and upon the nature of the used acid. Sullivan et al. [1] concluded that both diluted and highly concentrated acids, ranging from ambient temperature to 130 ºC, cause enormous iron corrosion. It is a challenge for mankind to achieve perfection in corrosion control issues. According to Poling [2], the latest survey of the worldwide anti-corrosion endeavors shows that the annual direct losses due to corrosion are about 1.4 trillion of a nation's GDP value. Earlier, according to Lorenz and Mansfeld [3], metals corrosion control was procured by the use of organic, inorganic and metallic coatings. During the 19th century [4-5], simple organic compounds, such as acetylenes, alcohols, ketones, amines, and some nitro compounds [1-6], played a vital role as corrosion inhibitors. In the 1960s, some polymeric compounds were found to be effective for corrosion inhibition. Recently, conducting polymers, such as polyanilines and polyvinylpyrrolidone (PVP), have been used as corrosion inhibitors compounds for iron/steel, brass, aluminum, and copper [6-9]. PVP derivatives, such as PVP-Oxime, proved to be biocompatible materials, and showed many applications in cosmetics, pharmaceuticals, bioprocessing identification of toxicity in wastewater, and as catalysts, bioscavengers, conjugated vaccines, and contact allergens [10-16]. Until now, PVP oxime has not been explored in corrosion inhibition studies. Herein, the authors have explored the capability of polyvinylpyrrolidone oxime (PVPO) for corrosion inhibition of a mild steel surface in 1 M H_2SO_4, through weight loss, electrochemical polarization, EIS, theoretical studies and SEM techniques, among others.

Materials and methods

Materials and synthesis of the inhibitor

Materials and sample preparation

The acidic medium of 1 M H_2SO_4 was prepared by dilution of analytical grade H_2SO_4 (minimum assay 98.0 %, Qualikem, India) of known molarity, with bidistilled water. The MS coupons of rectangular shape, with the composition given in Table 1, and the surface dimensions of 3.0 cm x 1.5 cm x 0.028 cm, were mechanically abraded and polished with a series of waterproof silicon carbide emery papers of 400, 600, 800, 1000, 1200, 1500 and 2000 grades, consecutively. Thereafter, they were washed with distilled water, degreased with acetone and, finally, dried in warm air, and made available for weight loss experiments.

Table 1. Composition of MS coupons.

Element	C	Si	Mn	S	P	Ni	Cu	Cr	Fe
Weight % (w/w)	0.14	0.03	0.32	0.05	0.20	0.01	0.01	0.01	Balance

Synthesis of the inhibitor compound - polyvinylpyrrolidone oxime (PVPO)

The principal ingredients, i.e., polyvinylpyrrolidone (PVP) (K-30, AR grade, Merck, India) and hydroxylamine hydrochloride (AR grade, Merck, India), were dissolved in a 1:2 ratio w/w, along with the addition of a minimum quantity of

70% aqueous ethanol required for the complete dissolution, taken in a 250 mL RB flask, and stirred with a magnetic stirrer for 45 min, followed by the addition of 5 mL of a 1 N NaOH solution, to adjust the pH value, and to increase the reaction rate. Meanwhile, a white PVPO precipitate was observed, which was filtered through a no. 42 Whatman filter, followed by washing with a 20% aqueous ethanol solution. After that, the precipitate was placed in a vacuum chamber, and dried for 48 hrs. Scheme 1 has been adopted for PVPO synthesis.

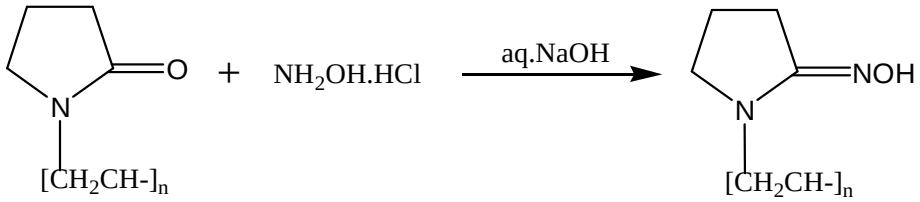

Scheme 1. PVPO synthesis.

Characterization of the synthesized PVPO

Fourier Transform Infrared Spectroscopy study (FTIR)

A simple and useful physical method for determining the functional groups on polymers is infra red spectroscopy. The FTIR spectra of PVPO fine powder was recorded by Perkin-Elmer FT-IR/RZX, and ranged from 4000 cm^{-1} to 400 cm^{-1}. The FTIR spectra of pure PVP (Fig. 1) shows a prominent peak at 1655.4 cm^{-1}, due to the presence of a carboxyl group attached to the pyrrolidone ring.

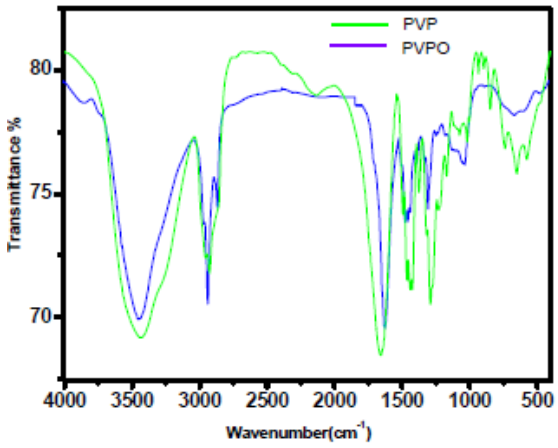

Figure 1. FTIR spectra of PVP and PVPO.

The stretching frequency, at 1430.18 cm^{-1} and 1459.62 cm^{-1}, was due to the C-N stretching of the PVP ring. The C-H bond stretching, at 2933.58 cm^{-1}, indicates the side chain (polyvinyl chain) while, in PVPO, the stretching frequency, at 1612.07 cm^{-1}, confirms the presence of the C=N stretching, which is at a lower frequency than in PVP. The stretching frequency at 3442.26 cm^{-1} shows the presence of the -OH group attached to the N atom in PVPO. Other peaks are approximate at similar frequency ranges, as in PVP.

Proton NMR

^{1}H NMR gives information about the protons number, types and environment. The proton NMR spectra of PVPO were monitored in deuterium on a DPX-dix 500 MHZ Bruker advance spectrometer, using TMS as an internal reference.

H (a) and H (b) protons had triplet signals, at 3.3-3.6 ppm, and got merged with each other. H (c) and H (d) protons had multiplet signals, at 1.1-2.4 ppm, and got merged with each other. The H (e) proton signal of the hydroxyl group that was attached to nitrogen appears downfield, at 4.64 ppm.

Experimental techniques

Weight loss technique

The MS coupons, with the dimensions of (3 x 1.5 x 0.028) cm^3, after accurately weighing, were immersed in 200 mL of 1 M H_2SO_4, in the inhibitor absence and presence, at different concentrations (200, 400, 600, and 1000 ppm), and at different temperatures (303 K, 313 K and 323 K).

Each experiment was carried out in triplicate, to get results reproducibility, using a freshly prepared solution. The temperature was thermostatically controlled during 6 h of immersion, after which the specimens were taken out and washed with distilled water.

The loosely adhered corrosion product was scared off with rubber cork and, thereafter, the specimen was rinsed with acetone, dried and, again, accurately weighed. The corrosion rate in mmpy was calculated from the following relation:

$$Corrosion\ rate\ (CR) = \frac{534 \times \Delta W}{DAT} \qquad (1)$$

where D is mild steel density (7.86 gcm^{-3}), ΔW is MD weight loss (mg), T is the immersion time (in hours) and A is the total area of the mild steel coupon (cm^2).

The percentage inhibition efficiency (η) was measured using the following equation:

$$\eta\ \% = \frac{CR^0 - CR}{CR^0} \times 100 \qquad (2)$$

where CR^0 and CR are MS corrosion rate in the 1 M H_2SO_4 uninhibited and inhibited solutions.

Electrochemical measurements

For the electrochemical studies, it was used a potentiostat/Galvanostat (PGSTAT204), Autolab, Netherland, with a FRA32M module, which was controlled by NOVA 1.11 software. It was used a Pyrex glass cell with three electrodes, consisting of a mild steel coupon as working electrode(WE), graphite as counter electrode, and silver-silver chloride as reference electrode, connected, via a Luggin capillary, for electrochemical polarization. The MS coupon area of 1 cm^2 was attached to a holder, and the Luggin probe tip was made very close to the MS surface. The working electrode was kept in a 1 M H_2SO_4 corrosive solution for sufficient time to get open circuit potential (OCP) attainment. Potentiostatic polarization studies were performed in PVPO absence and

presence, in the potential range of ±0.25 V, with a constant sweep rate of 1.0 mV /s. The electrochemical parameters, including corrosion rate (CR), corrosion potential (E_{corr}), cathodic and anodic Tafel slopes (β_c and β_a) and corrosion current density (I_{corr}), have been computed. The inhibition efficiency was calculated using the following equation:

$$\eta\,\% = \frac{i^{o}_{corr} - i_{corr}}{i^{o}_{corr}} \times 100 \qquad (3)$$

where i_{corr} and i^{o}_{corr} are the corrosion current densities, respectively, in the uninhibited and inhibited solutions for MS. The electrochemical impedance spectroscopy (EIS) was performed in the frequency range of 100 kHz to 0.01 Hz, using an AC 5 mV signal. The parameters obtained from the EIS study are charge transfer resistance (R_{Ct}), maximum frequency (f_{max}), electric double-layer capacitance (C_{dl}) and inhibition efficiency (η%), which were calculated using the following relations:

$$C_{dl} = \frac{1}{2\pi f_{max} R_{CT}} \qquad (4)$$

$$\eta\% = \frac{R_{CT} - R^{0}_{CT}}{R^{0}_{CT}} \times 100 \qquad (5)$$

where R_{CT} ad R^{0}_{CT} are the charge transfer resistance in PVPO presence and absence, respectively.

Scanning electron microscopy (SEM)

A scanning electron microscope, with a Zeiss Ultra 55 Model, at 3 kV, was used to investigate the specimens' morphology. MS coupons were immersed in the 1 M H_2SO_4 test solution, in the inhibitor absence and presence, with 1000 ppm concentration, for 6 h, at 303 K. After the experiment completion, these coupons were taken out, abraded and polished with different grades of emery papers. Then, all the specimens were washed with distilled water, and then with acetone, dried and placed in a desiccator, until they were shifted to the SEM chamber, for surface morphology.

Quantum chemical calculations

A quantum chemical study has been made, to look into the relationship between the compound's molecular structure, electronic properties and the extent of its corrosion inhibiting ability. The quantum chemical parameters were calculated using a HyperChem Professional 8.0 package (Hypercube Inc., USA), considering AM1 (Austin Model1). The various quantum chemical descriptors, such as energy of the highest occupied molecular orbital (E_{HOMO}), energy of the lowest unoccupied molecular orbital (E_{LUMO}), their energy gap (that is, ΔEgap = E_{LUMO} - E_{HOMO}), dipole moment (μ), absolute electronegativity (χ), absolute hardness (η), and fraction of electrons (ΔN) available for transfer from the inhibitor to the iron surface, were computed by the application of the appropriate equations for a specific descriptor:

$$\eta = \frac{1}{2}(E_{LUMO} - E_{HOMO}) \qquad (6)$$

$$\chi = -\frac{1}{2}(E_{LUMO} - E_{HOMO}) \quad (7)$$

$$\Delta N = \frac{\chi_{Fe} - \chi_{inh}}{2(\eta_{Fe} + \eta_{inh})} \quad (8)$$

where χ_{inh} and η_{inh} denote PVPO's electronegativity and hardness, respectively, whereas η_{Fe} and χ_{inh} denote metal's electronegativity and hardness, respectively.

Results and discussion

Weight loss measurements

Effect of concentration and temperature

The variation of the inhibition efficiency at different PVPO concentrations in 1 M H_2SO_4 is given in Table 2 and Fig. 2. The figure shows that PVPO efficiently inhibited mild steel corrosion in a 1 M H_2SO_4 solution. It is obvious from the inhibition efficiency (η) value that the corrosion rate decreased with increasing PVPO concentrations, and Table 2 also shows that the inhibition efficiency (η) increased at higher concentrations, reaching a maximum value of 83.16%, at 303 K, with 1000 ppm of PVPO. This may be due to PVPO adsorption onto the MS surface through non-bonding electron pairs of nitrogen atoms and oxygen atoms [17-19]. In PVPO absence, CR is 365.18 mmpy, while in PVPO presence, at 303 K, with 1000 ppm, CR values are reduced to 61.49 mmpy.

Table 2. Corrosion rate and inhibition efficiency at different PVPO concentrations, and at 303 K, 313 K and 323 K, using weight loss method.

Inhibitor	Concentration (ppm)	*CR* (mmpy) at 303 K	*η*%	*CR* (mmpy) at 313 K	*η*%	*CR* (mmpy) at 323 K	*η*%
	Blank	365.18	-	598.44	-	1096.22	-
PVP-Oxime	200	136.72	62.56	263.85	55.91	677.24	38.22
	400	109.55	70.00	242.18	59.53	633.39	42.22
	600	89.61	75.46	213.22	64.37	571.34	47.88
	1000	61.49	83.16	173.00	71.09	504.26	54.00

To investigate the temperature effect, (Abboud et al. [20]), another tool that has been used to explain the corrosion inhibition mechanism (with and without PVPO) is also shown in Table 2 and Fig 2. The data obtained due to the temperature effect (at different ranges: 303 K, 313 K, and 323 K) on the MS surface in 1 M H_2SO_4, after 6 h of immersion, are listed in Table 2. It may be seen from the weight loss experiments that an increase in temperature may decrease the interaction between the MS sheet and the corrosive medium; that is why the corrosion rate increases, as pre-described by Dahiya et al. [21]. In acidic media, higher temperatures increase the rate of metal dissolution with the inhibitor adsorption. As the temperature increases from 303 K to 323 K, the inhibition efficiency (η %) decreases. So, there is minimum efficiency (54 %) at higher temperatures, i.e., at 323 K, and maximum efficiency (83.16%) at lower temperatures, i.e., 303 K, and at 1000 ppm (Daoud et al. [22]). The decrease in

I.E. % (η) value may be due to PVPO desorption initiation [23-24] from the MS surface, at higher temperatures.

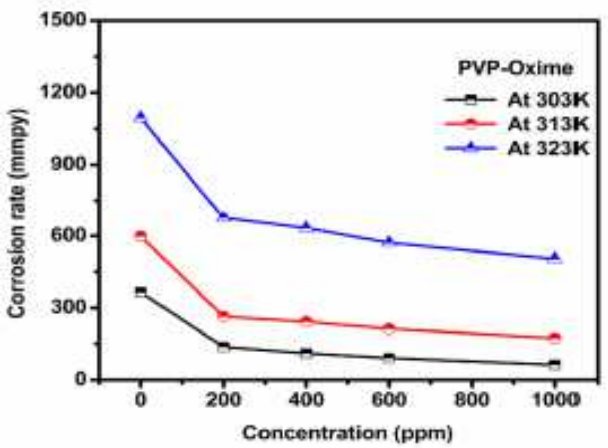

Figure 2. Corrosion rate versus inhibitor concentrations (200 ppm, 400 ppm and 1000 ppm), at different temperatures.

Electrochemical measurements

Potentiostatic polarization studies

Potentiostatic polarization studies were carried out, in order to find out the effect of the enhancement in PVPO concentration level on MS anodic and cathodic polarization curves, in a 1 M H_2SO_4 solution, at 303 K. The findings are represented in Fig. 3 (polarization plots), as well as in Table 3 (Tafel parameters), in the absence and presence of different concentrations (200 ppm - 1000 ppm) of the compound. Tafel extrapolation of both anodic and cathodic polarization curves depicts electrochemical kinetic parameters, such as anodic and cathodic Tafel slopes, βa and βc ($mVdec^{-1}$), respectively, corrosion potential, E_{corr} (mV), corrosion current density, I_{corr}, (μAcm^{-2}), inhibition efficiency (η%), which all are placed in Table 3.

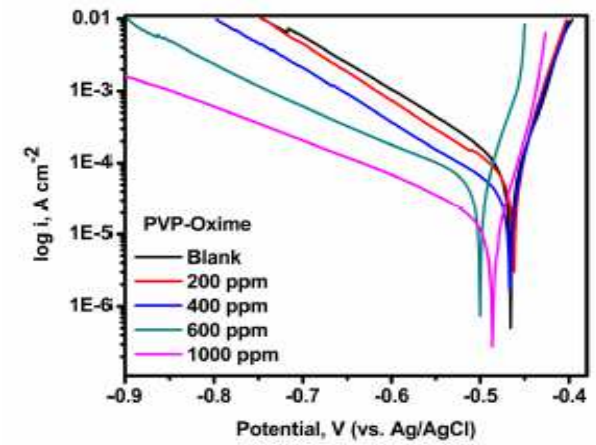

Figure 3. Potentiostatic polarization curves for MS in 1 M H_2SO_4, with different PVPO concentrations, at 303 K.

These electrochemical parameters are helpful to assess the inhibitor type: anodic, cathodic or mixed type. There is a marginal shift in the E_{corr} values, which indicates that PVPO might have predominantly acted as a mixed inhibitor (Li [24]). The values of these Tafel slopes were also found to vary with PVPO concentration. This, again, clarifies that the studied compound controlled both anodic and cathodic reactions and, thus, behaved as a mixed type inhibitor. From Fig. 3, it is clearly observed that the current density (I_{corr}) decreases from 63.46 (μAcm^{-2}) to 16.99 (μAcm^{-2}), with an increase in PVPO concentration from 200 ppm to 1000 ppm. This indicates a modification of anodic, as well as cathodic, half reactions, suggesting that PVPO mainly inhibits the corrosion process. This decrease in the corrosion process may be attributed to the covering of the metal surface with a monolayer, due to the adsorbed PVPO molecules onto the metal surface, through a free electron pair from PVPO oxygen and nitrogen atoms (Zhang [25]). The I.E. was calculated from I_{corr} values (Ravichandran et al. [26]), and it is also listed in Table 3. It was found to be maximum (i.e., 88.39%) with 1000 ppm concentration, at 303 K.

Electrochemical impedance spectroscopy (EIS) measurements

For the sake of weight loss and polarization techniques authentication, MS corrosion behavior in 1 M H_2SO_4, in the absence and presence of different PVPO concentrations, was investigated by electrochemical impedance spectroscopy, at 303 K, and the findings are shown in Fig. 4 (Nyquist plots). Double-layer capacitance (C_{dl}), charge transfer resistance (R_{CT}), surface coverage (Θ) and I.E. (η%) values are shown in Table 4.

At various PVPO concentrations, R_{CT} values increased from 62.53 Ω cm^2 to 119.20 Ω cm^2, whereas C_{dl} values get decreased from 159 μFcm^{-2} to 83 μFcm^{-2}, going from 200 ppm to 1000 ppm, which may be due to the increase in the thickness of the double layer (Mansfeld et al. [27]) and/or to the decrease in the dielectric constant. Consequently, the rate of the metal dissolution lowered down [28-29].

Table 3. Polarization parameters for MS in 1 M H_2SO_4, in PVPO absence and presence, at varying concentrations.

Inhibitor	C (ppm)	β_a (mV dec^{-1})	β_c (mV dec^{-1})	E_{corr} (mV vs. Ag/AgCl)	I_{corr} (μA cm^{-2})	CR (mmpy)	η (%)	Θ
PVPO	Blank	150.60	37.60	466	146.46	1.702	-	-
	200	128.74	26.47	462	63.46	0.737	56.67	0.5667
	400	142.25	28.65	466	47.19	0.548	67.78	0.6778
	600	131.80	28.23	500	37.25	0.433	74.56	0.7456
	1000	196.12	31.62	486	16.99	0.197	88.39	0.8839

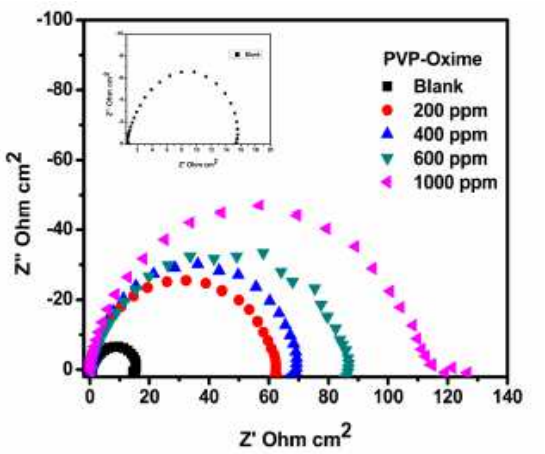

Figure 4. Nyquist plots for MS in 1 M H_2SO_4, obtained at 303 K, and at different PVPO concentrations.

Table 4. EIS parameters for MS in 1 M H_2SO_4, in the absence and presence of different PVPO concentrations.

Inhibitor	C (ppm)	R_{CT} (Ω cm^2)	$f_{max.}$ (Hz)	C_{dl} (μF cm^{-2})	Θ	η %
Blank	-	14.909	28.11	380	-	-
PVP-Oxime	200	62.53	15.99	159	0.7616	76.16
	400	69.31	21.21	108	0.7849	78.49
	600	87.20	21.21	86	0.8290	82.90
	1000	119.20	15.99	83	0.8749	87.49

Fig. 4 clearly shows that the diameter of Nyquist plots gets broadened at higher PVPO concentrations, which suggests that PVPO adsorption onto the MS surface blocked its active sites, and enhanced the metal corrosion resistance [30-31]. I.E. (η %) value increased from 76.16% to 87.49%, with an increase in PVPO concentration, from 200 ppm to 1000 ppm, which shows the improved protection of the MS surface at 1000 ppm. The experimental results obtained from the potentiostatic polarization, EIS, as well as the weight loss findings, agree well with each other, and prove that PVPO inhibits corrosion for MS in 1 M H_2SO_4.
Fig. 5 shows the equivalent circuit model for the EIS study, where n = value of the exponent of the constant phase element and R_P (Ohm cm^2) = polarization resistance (also referred to as the charge transfer resistance).

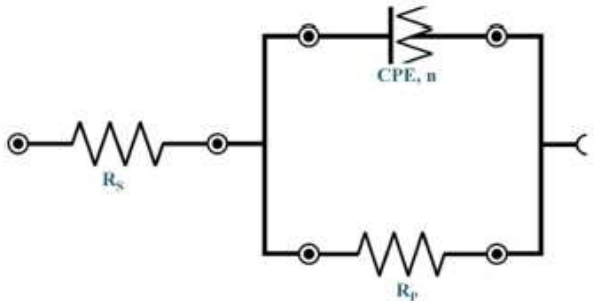

Figure 5. Equivalent circuit model for PVPO.

Adsorption and thermodynamic studies

Adsorption is an essential step of the inhibition mechanism, which gives basic information on the nature of the interaction between the metal corroding surface and the adsorbed molecules. Reports show that, mostly, the inhibitor retards both anodic and cathodic corrosion reactions [32-33]. So, to describe PVPO adsorption onto the MS surface, several adsorption isotherms, such as Freundlich, Langmuir, Temkin and Flory–Huggins isotherms, were tested and, to find a good regression value, Langmuir adsorption isotherm was found to be the best fitted isotherm.

The Langmuir adsorption equation is:

$$\frac{C}{\theta} = \frac{1}{K_{ads}} + C \qquad (9)$$

where θ is the surface coverage, C is the organic inhibitor concentration and K_{ads} is the equilibrium constant. The results also reveal that the plots of C/θ versus C offer good linear regression ($R^2 \geq 0.99$), close to 1. From this (Fig. 6), it is concluded that there is the formation of a monolayer on the heterogeneous MS surface, and that there are no interactions among the adsorbed PVPO molecules [34-35].

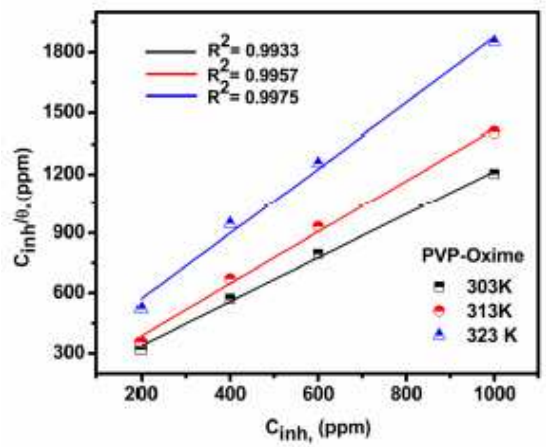

Figure 6. Langmuir isotherm for PVPO adsorption in 1 M H_2SO_4, at different temperatures.

The standard free energy of adsorption (ΔG°_{ads}) for the mild steel surface is related to K, with the following equation:

$$K = \frac{1}{55.5} \exp\left(-\frac{\Delta G^{\circ}_{ads}}{RT}\right) \qquad (10)$$

where R is the universal gas constant, T is the thermodynamic temperature and the value of 55.5 (mol L^{-1}) is the water concentration. ΔG°_{ads} values up to -20 kJ mol^{-1} are associated with the electrostatic interaction between any inhibitor and the charged metal electrode surface (physical adsorption), and values up to -40 kJ mol^{-1} or higher indicate charge transfer sharing between the inhibitor and the charged metal surface [33, 36-37]. For PVPO, ΔG°_{ads} was calculated as -23.52 kJ

mol^{-1}, -24.10 kJ mol^{-1} and -23.13 kJ mol^{-1}, at 303 K, 313 K and 323 K, respectively (Table 5). ΔG°_{ads} negative value indicates the presence of an interaction between PVPO molecules and the MS surface, which signifies the occurrence of physical adsorption type, along with slight chemical adsorption too.

Table 5. Thermodynamic parameters for MS in 1 M H_2SO_4, at 303, 313 and 323 K.

Temperature (K)	$1/K_{ads}$ (M)	ΔG°_{ads} (kJ mol^{-1})
303	119.9	- 23.52
313	129.28	- 24.10
323	247.06	- 25.13

Scanning electron microscopy (SEM) study

Figs. 7a and 7b show the SEM images of the polished mild steel surface without and with PVPO, at the magnification of x500, with 1000 ppm, and at 303 K, respectively, both immersed in a 1 M H_2SO_4 solution, for 6 h. The SEM image in Fig. 7a shows that the surface was rough, porous, loose and severely corroded, with a granular structure. In contrast, Fig. 7b reveals the formation of a dense, smooth, crack free protective film by PVPO onto the metal surface, which considerably inhibits the corrosion in an acidic medium. Hence, PVPO provides a good inhibition onto the mild steel surface, in a 1 M H_2SO_4 solution.

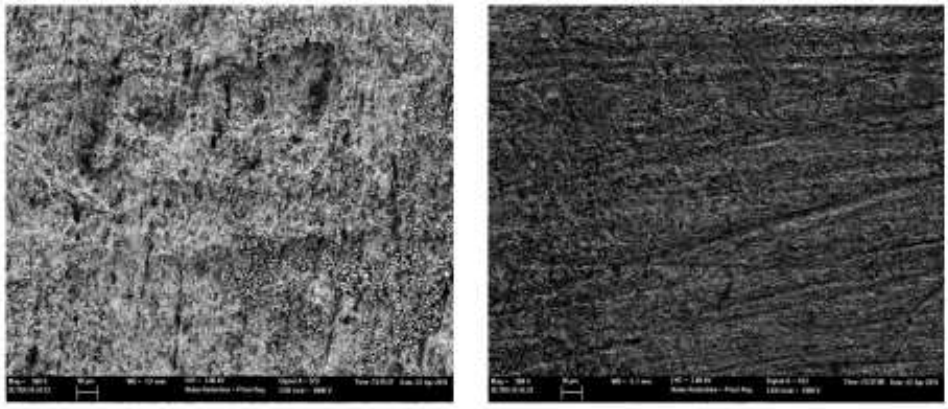

Figure 7. SEM micrographs of the MS surface in 1 M H_2SO_4. (**a)** Without PVPO; **(b)** at 1000 ppm of PVPO in 1 M H_2SO_4, at 303 K.

Corrosion inhibition mechanism complemented by quantum chemical study

We attempted to interpret the main causes responsible for the reactivity of the synthesized PVPO towards a metal surface, and to analyze its capability to donate and accept electrons from the MS surface. PVPO optimized structure (Table 6 and Fig. 8a) gives an idea about the planarity/non-planarity of the molecular structure. On the basis of this, we can conclude that a structure with high planarity is generally found to exhibit higher I.E. %, because of the coulombic association between the adsorbing inhibitor molecule and the MS

surface [38-39], while the corresponding electron density present on PVPO HOMO and LUMO surfaces is shown in Fig. 8(b) and Fig. 8(c), respectively.

Table 6. PVPO quantum chemical parameters.

Quantum parameters→	E_{HOMO}	E_{LUMO}	η	χ	ΔN	ΔE_T	μ (D)
PVPO	-9.508	-1.493	4.008	5.500	0.187	-1.002	1.183

HOMO frontier molecular orbital distribution (Fig. 8b) gives important information on the segment of the investigated molecule that can act as an electron donor during its adsorption onto the MS surface (Shaban [40]). Generally, a molecule with a high E_{HOMO} value indicates the inhibitor high electron donating capability to the MS surface, thus providing high inhibition efficiency, while a lower E_{LUMO} value is related to the studied compound capacity to accept electrons [41-42]. The energy difference *(*ΔE) of E_{LUMO} and E_{HOMO} is another important descriptor that can be used to know the reactivity and inhibition properties of the studied compound. According to Gomez et al. [43], low energy difference (ΔE), efficiency and chemical reactivity values, in PVPO case, indicate that it acts as a good corrosion inhibitor.

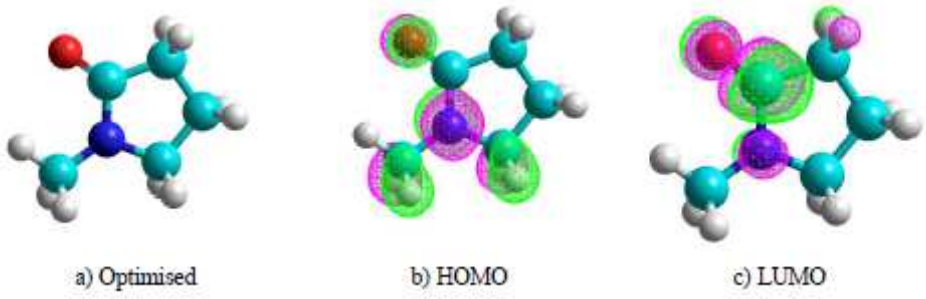

Figure 8. (a) PVPO optimized structure; (**b)** PVPO HOMO; and **(c)** PVPO LUMO.

In addition to the above information, the global electronegativity (χ) value shows (Table 6) that PVPO has the susceptibility to contribute with its electrons towards metal. The energy change (ΔE_T) accompanies the electron transfer from an inhibiting compound to the iron atom, which can be used to predict the favorability of donor–acceptor interactions between the Fe atom and the inhibitor (Gomez et al. [43]). Also, the studied compound with high dipole moment value (μ) possesses a preferred tendency to donate its electron density towards the metal surface, proving to be a good inhibitor (Dahiya et al. [44]).

Conclusion

Polyvinylpyrrolidone Oxime (PVPO) was synthesized using PVP, to study its corrosion controlling behavior for mild steel (MS) in 1 M H_2SO_4, at different concentrations and temperatures. PVPO acted as quite a good inhibitor for

controlling MS corrosion in a 1 M H_2SO_4 solution, with 83.16 % and 88.39 % inhibition efficiency (I.E.), studied by weight loss and polarization methods, respectively. The I.E. was enhanced at higher PVPO concentrations, but fell down at higher temperatures. Polarization curves show that PVPO acts as a mixed-type inhibitor. The measurements from Nyquist plots show that R_{ct} value increased, and C_{dl} value declined in PVPO presence, which confirms the increase in double layer thickness. Results obtained from potentiostatic polarization technique, EIS and weight loss techniques are in good agreement. PVPO adsorption obeys the Langmuir adsorption isotherm.The thermodynamic parameters indicate both physisorption, with slight chemisorptive behavior between metal and PVPO. Quantum chemical calculations showed that PVPO interacts with the metal, attaining electrostatic interactions, and the study accords well with experimental results, revealing that PVPO has proper moiety to decrease the corrosion reaction rate. The SEM images also verify that, with PVPO, the MS surface is smooth and less cracked compared to that in the uninhibited solution, forming a smooth and protective layer through the adsorption over the MS surface.

Acknowledgements
We are grateful to Deenbandhu Chhotu Ram University of Science and Technology, Murthal, Sonipat, Haryana, for sparing the necessary facilities.

References

1. Sullivan DS, Strubelt CE, Becker KW. High temperature corrosion inhibitors, US Patent, 7(1977) 4028268.
2. Poling GW. J Electrochem Soc. 1967;114:1209.
3. Lorenz WJ, Mansfeld F. Determination of corrosion rates by electrochemical DC and AC methods. Corros Sci. 1981;21:647.
4. Elewady GY, Mostafa HA. Ketonic secondary Mannich bases as corrosion inhibitors for aluminium. Desalination. 2009;247:573-582.
5. Mengoli G, Musiani M, Pagura MC, et al. Inhibition Performance of a New Series of Mono-/Diamine-Based Corrosion Inhibitors for HCl Solutions. Corros Sci. 1991;32:743.
6. Abed Y, Hammouti B, Touhami F, et al. Poly (4-vinylpyridine) (P4VP) as Corrosion Inhibitors of Armco Iron in Molar Sulphuric Acid Solution. Bull Electrochem. 2001;17:105-108.
7. Abdallah M, Megahed HE, El-Etre AY, et al. Polyamide compounds as inhibitors for corrosion of aluminium in oxalic acid solution. Bull Electrochem. 2004;20:277.
8. Muralidharan S, Phani KLN, Pitchumani S, et al. Polyamino benzoquinone polymers: A new class of corrosion inhibitors for mild steel. J Electrochem Soc. 1995;142:1478.

9. Umoren SA. J Green Chemistry Letters and Reviews. Coconut coir dust extract: a novel eco-friendly corrosion inhibitor for Al in HCl solutions, Appl Polym Sci. 2011;119:2072.
10. Kros A, Gerritsen M, Sprakel VSI, et al. Silica-based hybrid materials as biocompatible coatings for glucose sensors. Sensors Actuat B: Chem. 2001;81(1):68-75.
11. Shi L, Miller C, Karin DC, et al. Effects of mucin addition on the stability of oil–water emulsions. Colloid Surface B. 1999;15: 303-312.
12. Alexandridis P, Hatton TA. Poly (ethylene oxide) poly (propylene oxide) poly (ethylene oxide) block copolymer surfactants in aqueous solutions and at interfaces: thermodynamics, structure, dynamics, and modeling. Colloid Surf. 1995;96:1.
13. Chu B. Structure and Dynamics of Block Copolymer Colloids. Langmuir. 1995;11:414.
14. Patel B, Sexena A. Bioscavengers for the protection of humans against organophosphate toxicity. Chem Biol Interact. 2005;157-158:167-171.
15. Lees A, Sen G, Lopez A, et al. Versatile and efficient synthesis of protein polysaccharide conjugate vaccines using aminooxy reagents and Oxime chemistry. Vaccine. 2006;24:716-729.
16. Nilsson AM, Bergström, Luthman K, et al. An α, β-unsaturated oxime identified as a strong contact allergen: Indications of antigen formation via several pathways. Food ChemToxicol. 2005;43:1627-1636.
17. Verma CB, Singh P, Quraishi MA. A thermodynamical, electrochemical and surface investigation of Bis (indolyl) methanes as Green corrosion inhibitors for mild steel in 1 M hydrochloric acid solution. JAAUBAS. 2016;21:24-30.
18. Gopiraman M, Selvakumaran N, Kesavan D, et al. Adsorption and corrosion inhibition behaviour of N-(phenylcarbamothioyl) benzamide on mild steel in acidic medium. Prog Org Coat. 2012;73:104-111.
19. Dahiya S, Lata S, Kumar R, et al. Comparative performance of Uroniums for controlling corrosion of steel with methodical mechanism of inhibition in acidic medium. Part 1. J Mol Liq. 2016;221:124-132.
20. Abboud Y, Abourriche A, Saffaj T, et al. A novel azo dye, 8-quinolinol-5-azoantipyrine as corrosion inhibitor for mild steel in acidic media. Desalination. 2009;237:175.
21. Dahiya S, Kumar P, Lata S, et al. An exhaustive study of a coupling reagent (1-(3-dimethylaminopropyl)3-ethylcarbodiimide hydrochloride) as corrosion inhibitor for steel. IJCT. 2017;24:327-335.
22. Daoud D, Douadi T, Hamani H, et al. Corrosion inhibition of mild steel by two new S-heterocyclic compounds in 1 M HCl: Experimental and computational study. Corros Sci. 2015;94:21-37.
23. Malik R, Dahiya S, Lata S. An experimental and quantum chemical study of removal of utmostly quantified heavy metals in wastewater using coconut husk: A novel approach to mechanism. Int J Biol Macromol. 2017;98:139-149.

24. Li X, Deng S, Fu H. Adsorption and inhibition effect of vanillin on cold rolled steel in 3.0 M H_3PO_4. Prog Org Coat. 2010;67:420-426.
25. Zhang K, Xu B, Yang W, et al. Halogen-substituted imidazoline as corrosion inhibitors for mild steel in hydrochloric acid solution. Corros Sci. 2015;90:284-295.
26. Ravichandran R, Nanjundan S, Rajendran N. Effect of benzotriazole derivatives on the corrosion and dezincification of brass in neutral chloride solution. J Appl Electrochem. 2004;34:1171.
27. Mansfeld F, Kending MW, Tsai S. Recording and analysis of AC Impedance data for corrosion studies. II. Experimental and results. Corrosion. 1982;38 (11):570-580.
28. Gomez B, Likhanova NV, Dominguez-Aguilar MA, et al. Quantum Chemical Study of the Inhibitive Properties of 2-Pyridyl-Azoles. J Phys B. 2006;110:8928-8934.
29. Kumar R, Chahal S, Dahiya S, et al. Experimental and theoretical approach to exploit the corrosion inhibition activity of 3-formylchromone derivatives on mild steel in 1 M H_2SO_4. Corros Rev. 2017.
30. Tang Y, Zhang F, Huc S, et al. Novel benzimidazole derivatives as corrosion inhibitors of mild steel in the acidic media. Part I: Gravimetric, electrochemical, SEM and XPS studies. Corros Sci. 2013;74:271.
31. Verma C, Quraishi MA, Olasunkanmi LO, et al. L-Proline-promoted synthesis of 2-amino-4-arylquinoline-3-carbonitriles as sustainable corrosion inhibitors for mild steel in 1 M HCl: experimental and computational studies. RSC Adv. 2015;5:85417.
32. Dahiya S, Lata S. Adsorption and Thermodynamics Behaviors of Ferroin [tris (1,10-phenanthroline Iron(II) Sulphate Complex] as Corrosion Inhibitor for Mild Steel in Acidic Medium. ACSJ. 2016;10(2):1-11.
33. Donahue FM, Nobe K. Theory of Organic Corrosion Inhibitors Adsorption and Linear Free Energy Relationships. Electrochem Soc. 1965;112:886–891.
34. Tourabi M, Nohair K, Traisnel M, et al. Electrochemical and XPS studies of the corrosion inhibition of carbon steel in hydrochloric acid pickling solutions by 3,5-bis(2-thienylmethy)-4-amino-1,2,4-triazloe. Corros Sci. 2013;75:123-133.
35. Keles H, Keles M, Dehri I, et al. The inhibitive effect of 6-amino-mcresol and its Schiff base on the corrosion of mild steel in 0.5 M HCl medium. Mater Chem Phys. 2008;112:173-179.
36. Ashassi H, Shaabani B, Seifzadeh D. Corrosion inhibition of mild steel by some Schiff base compounds in hydrochloric acid. Appl Surf Sci. 2005;239: 154-164.
37. Yuce AO, Mert BD, Kardaş G, et al. Electrochemical and quantum chemical studies of 2-amino-4-methyl-thiazole as corrosion inhibitor for mild steel in HCl solution. Corros Sci. 2014;83:310-316.
38. Ebenso EE, Kabanda MM, Murulana LC, et al. Electrochemical and quantum chemical investigation of some azine and thiazine dyes as

potential corrosion inhibitors for mild steel in hydrochloric acid solution. Ind Eng Chem Res. 2012;51:12940–12958.
39. Bentiss F, Lagrenee M. Heterocyclic compounds as corrosion inhibitors for mild steel in hydrochloric acid medium - correlation between electronic structure and inhibition efficiency. J Mater Environ Sci. 2011;2:13-17.
40. Shaban SM. *N*-(3-(Dimethyl benzyl ammonio) propyl) alkanamide chloride derivatives as corrosion inhibitors for mild steel in 1 M HCl solution: experimental and theoretical investigation. RSC Adv. 2016;6:39784-39800.
41. Pearson RG. Absolute electronegativity and hardness. Application to inorganic chemistry. 1988;27:734-740.
42. Martinez S. Inhibitory Mechanism of mimosa tannin using molecular modeling and substitutional adsorption isotherm. Mater Chem Phys. 2003;77:97-102.
43. Gomez B, Likhanova NV, Dominguez MA, et al. Quantum chemical study of the inhibitive properties of 2-pyridyl-azoles. J Phys Chem B. 2006;110:8928-8934.
44. Dahiya S, Lata S, Kumar P, et al. A descriptive study of corrosion inhibition by aloe extract in acidic medium. Corros Rev. 2016;34:241-248.